International Journal of Pharmaceutics 639 (2023) 122965

Contents lists available at ScienceDirect

International Journal of Pharmaceutics

journal homepage: www.elsevier.com/locate/ijpharm

Ameliorating the antiparasitic activity of the multifaceted drug ivermectin through a polymer nanocapsule formulation

Zilyane Cardoso de Souza [a], Francisco Humberto Xavier Júnior [b], Irapuan Oliveira Pinheiro [a], Juliana de Souza Rebouças [c], Brenda Oliveira de Abreu [c], Paulo Roberto Ribeiro Mesquita [d], Frederico de Medeiros Rodrigues [d], Helenita Costa Quadros [e], Tiago Manuel Fernandes Mendes [f], Paul Nguewa [g], Silmara Marques Allegretti [f], Leonardo Paiva Farias [e], Fabio Rocha Formiga [a,h,*]

[a] *Graduate Program in Applied Cellular and Molecular Biology, University of Pernambuco (UPE), 50100-130 Recife, PE, Brazil*
[b] *Department of Pharmacy, Federal University of Paraíba (UFPB), 58051-900 João Pessoa, PB, Brazil*
[c] *Graduate Program in Health Sciences, University of Pernambuco (UPE), 50100-130 Recife, PE, Brazil*
[d] *Agricultural Technological Center of the State of Bahia (CETAB), 40170-110 Salvador, BA, Brazil*
[e] *Gonçalo Moniz Institute (IGM), Oswaldo Cruz Foundation (FIOCRUZ), 40296-710 Salvador, BA, Brazil*
[f] *Departament of Animal Biology, State University of Campinas (UNICAMP), 13083-862 Campinas, SP, Brazil*
[g] *University of Navarra, Institute of Tropical Health, Department of Microbiology and Parasitology, IdiSNA (Navarra Institute for Health Research), 31009 Pamplona, Spain*
[h] *Aggeu Magalhães Institute (IAM), Oswaldo Cruz Foundation (FIOCRUZ), 50670-420 Recife, PE, Brazil*

ARTICLE INFO

Keywords:
Ivermectin
Poly(ε-caprolactone)
Nanocapsules
Drug delivery system

ABSTRACT

Ivermectin (IVM) is a potent antiparasitic widely used in human and veterinary medicine. However, the low oral bioavailability of IVM restricts its therapeutic potential in many parasitic infections, highlighting the need for novel formulation approaches. In this study, poly(ε-caprolactone) (PCL) nanocapsules containing IVM were successfully developed using the nanoprecipitation method. Pumpkin seed oil (PSO) was used as an oily core in the developed nanocapsules. Previously, PSO was chemically analyzed by headspace solid-phase microextraction coupled to gas chromatography/mass spectrometry (HS-SPME/GC–MS). The solubility of IVM in PSO was found to be 4266.5 ± 38.6 μg/mL. In addition, the partition coefficient of IVM in PSO/water presented a logP of 2.44. A number of nanocapsule batches were produced by factorial design resulting in an optimized formulation. Negatively charged nanocapsules measuring around 400 nm demonstrated unimodal size distribution, and presented regular spherical morphology under transmission electron microscopy. High encapsulation efficiency (98–100%) was determined by HPLC. IVM-loaded capsules were found to be stable in nanosuspensions at 4 °C and 25 °C, with no significant variations in particle size observed over a period of 150 days. Nanoencapsulated IVM (0.3 mM) presented reduced toxicity to J774 macrophages and L929 fibroblasts compared to free IVM. Moreover, IVM-loaded nanocapsules also demonstrated enhanced *in vitro* anthelmintic activity against *Strongyloides venezuelensis* in comparison to free IVM. Collectively, the present findings demonstrate the promising potential of PCL-PSO nanocapsules to improve the antiparasitic effects exerted by IVM.

1. Introduction

Ivermectin (IVM) is a macrocyclic lactone (Fig. 1) with high antiparasitic efficacy, presenting action against many nematodes, such as *Ascaris, Enterobius, Strongyloides* and filarial worms (Laing et al., 2017; Van Voorhis et al., 2015). Importantly, William C. Campbell and Satoshi Ōmura were credited for the development of IVM, and were awarded the Nobel Prize in Medicine in 2015. These scientists' work in the 1970s initiated a chain of events driving to the control of onchocerciasis, a neglected tropical disease. The effectiveness of IVM has been

Abbreviations: IVM, Ivermectin; PCL, poly(ε-caprolactone); PSO, pumpkin seed oil; HS-SPME-GC-MS, Headspace Solid-Phase Microextraction/Gas Chromatography with Mass Spectrometry detection; %EE, percent of encapsulation efficiency; PDI, polydispersity index; VOCs, Volatile Organic Compounds.

* Corresponding author at: Department of Immunology, Aggeu Magalhães Institute (IAM), Oswaldo Cruz Foundation (FIOCRUZ), Av. Prof. Moraes Rego, s/n, 50670-420 Recife, PE, Brazil.
E-mail address: fabio.formiga@fiocruz.br (F.R. Formiga).

https://doi.org/10.1016/j.ijpharm.2023.122965
Received 24 July 2022; Received in revised form 30 March 2023; Accepted 13 April 2023
Available online 20 April 2023

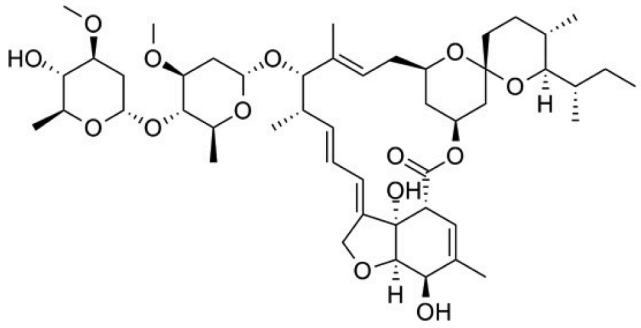

Fig. 1. Molecular structure of ivermectin.

demonstrated by the Onchocerciasis Control Programme (OCP) (Burnham and Mebrahtu, 2004). Furthermore, recent studies point to the potential of IVM as an antiviral agent, with demonstrated pre-clinical activity against pseudorabies virus (Lv et al., 2018), chikungunya (Varghese et al., 2016), West Nile virus (Yang et al., 2020) and more recently, *in vitro* activity against SARS-CoV-2, the causative agent of COVID-19 (Caly et al., 2020).

Despite the drug's demonstrated efficacy, critical issues have been associated with the currently available formulations of IVM in conventional dosage forms, i.e. tablets, capsules and suspensions. These forms do not offer optimal pharmacokinetic profiles, which limit its antiparasitic action (Formiga et al., 2021). In fact, the oral bioavailability of IVM is low mainly due to its poor water solubility (Takano et al., 2006). In addition, IVM binds to organic material in the intestine (Gokbulut et al., 2006). Since IVM is pumped back into the intestinal lumen by the P-glycoprotein present in the intestinal epithelium, this then reduces its antiparasitic activity (González-Canga et al., 2009). Furthermore, although IVM is widely used in the treatment of several parasitic diseases and is currently the drug of choice for strongyloidiasis, its application is restricted due to side effects. *Strongyloides* has one of the most complex autoinfective life cycles of the human-infecting intestinal nematodes, presenting potential lifelong infection and capacity to kill its host decades after initial infection into the intestinal lumen (Page et al., 2018). In fact, IVM is used in a dose of 0.15 mg/kg–0.2 mg/kg body weight for most of the parasitic infestations as oral tablet and is generally well tolerated (González-Canga et al., 2009). However, several authors have described neurological effects in children under the age of 5 or those who weight <15 kg, as well as in pregnant women, lactating women or in patients with central nervous system disorders (Ottesen and Campbell, 1994; Pacqué et al., 1991). In addition, some issues with IVM efficacy have produced variable cure rates. Amato-Neto et al. evaluated the action of IVM in rats infected with *Strongyloides venezuelensis*, reporting inconsistent cure rates varying from 55 to 98% (Amato-Neto et al., 1997). Similarly, in immunocompetent patients infected with *Strongyloides stercoralis*, cure rates associated with IVM varied between 55 and 100% (Bisoffi et al., 2013; Panic et al., 2014; Luvira and Watthanakulpanich, 2014). Another complicating factor is the repeated and often indiscriminate use of IVM that has led to treatment failure and the appearance of tolerance/resistance (Laing et al., 2017; Kaplan, 2012).

Therefore, novel formulation approaches are required to maximize the bioavailability of IVM. One promising strategy is to formulate IVM into nanocarriers to overcome limited bioavailability inherent in drugs with poor water solubility. In the field of nanomedine, nanosized drug carriers offer several advantages, namely: specific drug delivery, high metabolic stability, high membrane permeability, improved bioavailability, controlled release and long-lasting action (Onoue et al., 2014). In this context, a number of studies have developed formulations of IVM in micro- and nanoparticles, either using lipid nanocapsules (Ullio-Gamboa et al., 2017), chitosan-alginate nanoparticles (Ali et al., 2013), liposomes (Croci et al., 2016), poly(d,l-lactide) and poly-(ε-caprolactone) microspheres (Dorati et al., 2015),or poly (lactic-co-glycolic acid) (PLGA) micro- and nanoparticles (Ali et al., 2014; Camargo et al., 2010; Clark et al., 2004; Surnar et al., 2019).

Polymer nanocapsules (NCs), vesicular particles with submicrometric dimensions ranging from 10 nm to 1000 nm, are composed of an oily core surrounded by an ultrathin polymeric wall (Poletto et al., 2011).NCs are versatile systems capable of increasing the photo- and chemical stability of compounds, as well as modulating interactions between the cargo and cells, thereby reducing the adverse effects of drugs while increasing drug bioavailability (Frank et al., 2015). Although NC-based formulations have been developed to enhance the therapeutic efficacy of a variety of active compounds (Frank et al., 2015; Chaves et al., 2017; Chen et al., 2014), applying this delivery system to IVM has yet to be thoroughly investigated.

The present investigation sought to develop a novel IVM formulation based on poly(ε-caprolactone) (PCL) nanocapsules formulated with pumpkin seed oil (PSO). Interestingly, pumpkin seed-derived bioproducts have been previously described for their antiparasitic effects (Feitosa et al., 2013; Grzybek et al., 2016; Beshay et al., 2019). Herein, PSO was used as a biologically active core for nanocapsule formation, resulting in a feasible, stable and effective IVM nanoformulation that exhibits enhanced anti-nematode activity *in vitro*.

2. Material and methods

2.1. Materials

Poly(ε-caprolactone) (PCL, M_w = 14,000), ivermectin (cat. I8898), sorbitan monooleate (Span 80) and polysorbate 20 (Tween 20) were purchased from Sigma-Aldrich (São Paulo, Brazil). Pumpkin Seed Oil (PSO), derived from *Cucurbita pepo L.,* was obtained by pressing with evaporation temperature starting at 110 °C supplied by ACQ & GBM Comércio e Desenvolvimento Ltda (Brasilia, Brazil). Acetone and ethyl alcohol were purchased from Química Moderna (São Paulo, Brazil). For liquid chromatography, LiChrosolv® HPLC gradient grade acetonitrile was obtained from Merck (Darmstadt, Germany). Milli-Q® water was used in all experiments. All research was conducted in conformance with the National System for the Governance of Genetic Heritage and Associated Traditional Knowledge (SisGen, Brazil) under registration number AD56712.

2.2. Analysis of pumpkin seed oil

2.2.1. GC–MS analysis

One microlitre of oil was diluted in 1 mL of methanol and then agitated. Next, 1 μL of this mixture was injected in the GC–MS system (Shimadzu GCMS- QP2010 Plus high performance single quadrupole, Kyoto, Japan) in a split mode (split ratio of 1.0) chromatographic run at 250 °C. Volatile Organic Compounds (VOCs) were separated in a capillary column (Rxi-1 MS 100% dimethyl polysiloxane; 30 m × 0.25 mm ID × 0.25 μm, Restek, Bellefonte, USA) using helium (99.99%) as a carrier gas at a flow rate of 0.80 mL/min. The oven temperature varied as follows: first 40 °C, then warmed to 80 °C for 2 °C/min (hold 3 min), then 0.5 °C/min to 100 °C (hold 3 min), then 5 °C/min to 150 °C, then 10 °C/min to 300 °C (total time 94.0 min). The transfer line temperature was 250 °C, while quadrupole mass detector conditions consisted of an ion source temperature of 250 °C, employing electron impact ionization at 70 eV. The identification of VOCs was achieved by comparing GC retention times and mass spectra with those of the pure standard compounds. The annotation of VOCs was performed by comparing the obtained mass spectra with the NIST 147 Library Database and Kovats retention index (KI) values using a homologous series of n-alkanes C_8–C_{40} to compare with values reported in the literature for similar chromatographic columns. The percentage of individual peaks was achieved by peak area normalization measured without correction factors.

2.2.2. High resolution mass spectrometry (HRMS) analysis

One microliter of oil was diluted in 1 mL of methanol and then agitated. Next, 1 μL of this mixture was injected by direct infusion in an Agilent 1290 Infinity Binary LC system. The mobile phase used was 0.1% formic acid in methanol at flow rate of 0.1 mL/min. HRMS analysis was performed on an Agilent 6550 Accurate-Mass Q-TOF LC/MS system equipped with Agilent Jet Stream technology for electrospray ionization. Total ion spectra were collected over a mass range of 100–1000 *m/z* in positive and negative modes. The Q-TOF MS parameters used were an acquisition rate of 1.0 spectra/s, a drying gas - temperature of 250 °C, drying gas flow rate of 14.0 L/min, sheath gas temperature of 250 °C, sheath gas flow rate of 10.0 L/min, nebulizer gas pressure of 45 psi, skimmer voltage of 65 V, octopole RF of 750 V, fragmentor voltage of 150 V, capillary voltage of 3.0 kV and nozzle - Voltage of 350 V. Agilent MassHunter Workstation software was used for processing spectra, data acquisition and qualitative analysis. CEU Mass Mediator version 2.0 software was employed to search for compounds in different databases (Kegg, Metlin, LipidMaps and HMDB).

2.2.3. Determination of Hydrophilic-Lipophilic Balance (HLB)

A group of emulsions was prepared following the spontaneous emulsification method (Macedo et al., 2006) in accordance with a Hydrophilic-Lipophilic Balance (HLB) variation sheet, using values between 11.7 and 4.3 (Supplementary material, Table S3). A surfactant of lipophilic nature (Span 80; HLB = 4.3) and another of hydrophilic nature (Tween 20; HLB = 16.7) were used. The preparation consisted of injecting the oil phase containing Span 80, PSO 5%$_{w/w}$ and ethyl alcohol into an aqueous phase containing Tween 20 and water. The spontaneous emulsification process occurred immediately when the oil phase was slowly incorporated by syringe into the aqueous phase under magnetic stirring (80 rpm). After forming the emulsion, the organic solvent was removed using a rotary evaporator for 15 min (40 °C/80 rpm). The final volume was adjusted to 60 mL and aliquots of freshly prepared emulsions were stored at 25 °C and 4 °C.

2.3. Nanocapsule preparation

NCs were prepared using the nanoprecipitation method (Fessi et al., 1988) by mixing the organic and aqueous phases (Table 1). Thus, x_1 (50–200 mg) of pumpkin seed oil, x_2 (20–60 mg) of PCL, and 12 mg of Span® 80 were solubilized in 6 mL of acetone to produce the organic phase. This phase was gently injected dropwise in 7 mL of the aqueous phase containing 12 mg of Tween® 20 and homogenized for 20 min at 50 rpm at 25 °C (Fisher- Bioblock Scientific AM 3001 K, Illkirch, France). The obtained colloidal dispersion was concentrated by rotary evaporator for 40 min (200 rpm/40 °C/65 mBar) (BÜCHI Rotavapor R-125, Heating Bath B-491, Vacuum pump V-700, recirculating Chiller F-108, Flawil, Switzerland) to eliminate the solvent. The nanocapsules were stored at +4 °C for 24 h before characterization.

2.4. Optimization of nanoencapsulation process

To optimize the NC formulation process, two independent variables, namely the amount of PCL (x_1) and PSO (x_2), were tested using five different levels (−1.4, −1.0, 0.0, 1.0, 1.4) (Table 2) in empty NC formulations (drug-free), based on the experimental model proposed by Montgomery (Montgomery, 2012). Next, a new set of NC formulations was prepared incorporating IVM into oil phase (2–20 mg).

Table 1
Composition of nanocapsule formulations.

Phase	Composition
Organic phase	
Poly (ε-caprolactone)	x_1
Pumpkin seed oil	x_2
Acetone	6 mL
Span 80	12 mg
Aqueous phase	
Tween 20	12 mg
Milli-Q® water	7 mL

2.5. Nanocapsule characterization

2.5.1. Particle size

The hydrodynamic mean diameter and size distribution of the nanocapsule dispersions were determined at 25 °C by quasi-elastic light scattering using a Zetasizer Nano ZS90 analyzer (Malvern, UK), with a fixed scatter angle of 90°. Samples were diluted at 1:100 before analysis in Milli-Q® water. Each measurement was performed in triplicate.

2.5.2. Zeta potential

The surface charge of each NC formulation was determined by laser doppler electrophoresis (Zetasizer Nano ZS90, Malvern, UK). Nanocapsule dispersions were diluted (1:100) in NaCl at 1 mM. Values are presented as the mean of measurements performed in three replicate samples.

2.5.3. Nanocapsule morphology

The surface morphology of NCs was examined by transmission electron microscopy (TEM). For high-resolution imaging, nanocapsule samples were distributed across film-coated copper grids and 2% uranyl acetate contrast agent was added. After 24 h, micrographs were obtained under a JEM-1230 transmission electron microscope (JEOL, Peabody, MA, USA).

2.5.4. Long-term stability of optimized nanocapsule formulation

NC-IVM and NC-BL suspensions were kept at 4 °C and 25 °C protected from light for 180 days. Size, PDI, drug content and visual appearance were monitored during this period.

2.6. Analysis of IVM by HPLC

IVM concentrations were determined by high-performance liquid chromatography (HPLC) using an Agilent 1200 series analyzer equipped with a G1312A binary pump and a G1315D diode array detector (243 nm wavelength), G1316A thermostatted column, a G1322A degasser and a G1329A autosampler. Data processing was performed using Agilent Chemstation software. A Zorbax Eclipse column (Agilent Technologies Co., Ltd.) measuring 4.6 × 150 mm was filled with 5-μm particles. The mobile phase consisted of a solution containing 75% acetonitrile and 25% Milli-Q® water, with an injection volume of 20 μL pumped at a rate of 1,000 mL/min under a pressure of 51 bars at 35 °C. A calibration curve was obtained using a standard IVM solution (Sigma-Aldrich Brazil Ltda).

2.7. IVM solubility and partition coefficient

To determine IVM solubility in water and PSO, an excess quantity of the drug was added to both Milli-Q® (1 mL) and PSO (1 mL). Both solutions were kept under stirring for 24 h at 25 °C to ensure saturation.

Table 2
Variables and levels for definition of the experimental region towards nanocapsule production.

Independent Variable		*Level*		
x_i		−1.0	0	1.0
x_1	Poly(ε-caprolactone) (mg)	20	40	60
x_2	Pumpkin seed oil (mg)	50	125	200
Dependent Variable		*Desired response*		
Y	Size (nm)	Small		

Samples were then centrifuged at 15,100 *g* for 15 min (Microcentrifuge, K14-1215, KASVI, Brazil) to precipitate any insoluble drug fractions. The supernatants were filtered through a nylon filter (0.20 μm, Merck Millipore, Massachusetts, USA), diluted in acetonitrile, shaken in an ultrasonic bath for 5 min, and finally analyzed by HPLC (Xavier-Junior et al., 2018). The partition coefficient of IVM to PSO and water was determined using 750 μL of oil and 750 μL of Milli-Q® water mixed together in a properly closed, pre-shaken glass vial, left for 24 h at 25 °C. Next, 1.5 ± 0.1 mg of IVM was added to this mixture, followed by magnetic stirring for an additional 24 h. To promote separation between the aqueous and oil phases, the samples were then centrifuged for 5 min at 5000*g*. Subsequently, the aqueous and oil phases were carefully separated and centrifuged at 15,100*g* for 15 min to precipitate insoluble crystals from the drug. The supernatant from each separate phase was filtered and diluted as needed in acetonitrile, then mixed in an ultrasonic bath for 5 min. The resulting solutions were analyzed by HPLC as described above. Partition coefficients were determined as the logarithmic ratio between the solubilized drug concentration in each lipophilic and hydrophilic phase (logP).

2.8. Determination of encapsulation efficiency

To determine the encapsulation efficiency (EE%) of IVM into PCL-PSO nanocapsules, the ultrafiltration method was used to separate free and encapsulated IVM. Aliquots (400 μL) of nanosuspensions were added to Microcon® ultrafiltration units (Millipore, 10 kDa) and centrifuged at 3000*g* for 15 min. Next, 50 μL of ultrafiltered samples were added to microtubes containing 200 μL acetonitrile. For free-IVM quantification, this mixture was then centrifuged at 6000*g* for 15 min and placed in vials for HPLC analysis. To determine the total amount of IVM, 100 μL of nanocapsules were solubilized in 9900 μL of acetonitrile under vortexing for 10 min. Thereafter, samples were centrifuged at 6000*g* for 5 min and the supernatant was analyzed for IVM content by HPLC. Quantification was performed in triplicate, with encapsulation efficiency calculated as follows:

$$EE(\%) = \frac{[IVM]_{total} - [IVM]_{free}}{[IVM]_{total}} \times 100$$

2.9. Cytotoxicity assays

Murine L929 fibroblasts and J774 macrophages were used to evaluate the cytotoxicity of nanocapsules. Both cell lines were cultured in Dulbecco's Modified Eagle Medium (DMEM) supplemented with 10% fetal bovine serum (Cultilab, Campinas, Brazil) and 50 μg/mL gentamicin (Novafarma, Anápolis-GO, Brazil). Both cell lines were plated on 96-well culture plates at density of 1×10^4 cells/well, and maintained at 37 °C under 5% CO_2 for 24 h. Cells were exposed to IVM-loaded nanocapsules or free/non-encapsulated IVM at the concentrations of 0.3 mM and 0.03 mM, and then incubated for 72 h. Empty nanocapsules were also evaluated. DMEM was used as cell viability positive control, while 10 μM pararosaniline chloride (Sigma-Aldrich) was employed as a negative control (cell damage). Finally, 20 μL/well of AlamarBlue reagent (Invitrogen, Carlsbad, USA) was added. After 4 h, colorimetric readings were performed at 570 and 600 nm using a SpectraMAx 190 instrument (Molecular Devices, Sunnyvale, CA).

2.10. In vitro anthelmintic activity

Adult *Strongyloides venezuelensis* parasitic females were obtained as previously described (Rugai et al., 1954) and maintained in Wistar rats (*Rattus norvegicus*). All experimental protocols were approved by the Institutional Review Board for Animal Experimentation (CEUA/UNICAMP, protocol number 4794-1/2018) and performed in accordance with the ethical principles adopted by the National Council for Animal Experimentation (CONCEA).

For the *in vitro* assay, female worms were washed thrice in saline solution (0.9% NaCl) after collection. Two females were added per well on a 24- well plate containing four concentrations of each treatment (IVM or NC-IVM): 120 μg/ml; 60 μg/ml; 30 μg/ml and 15 μg/ml. Blank nanocapsules (NC-BL) were also added to wells as a negative nanoformulation control. An additional control group was included in the absence of any treatment. Parasites were incubated at 37 °C under a 5% CO_2 atmosphere for 7 days. Readings were taken at 1 h, 3 h, 5 h, 24 h, 48 h, 3 days, 4 days, 5 days, 6 days, and 7 days. Worms lacking motility were considered dead, with events recorded in survival curves (Kaplan-Meier). The assay was performed independently three times.

2.11. Statistical analysis

Statistical analyses were performed using Graphpad Prism v5.0 software (San Diego, USA) and Statistica software (version 7.0, StatSoft Inc., USA). Nanoparticle optimization data were analyzed by one-way variance analysis (ANOVA) and Tukey's post hoc test. Results were expressed as mean ± standard error and considered statistically significant when $p < 0.05$. The effects of treatment on adult worms were recorded by Kaplan-Meier survival curves, with p values calculated using the log-rank (Mantel-Cox) test.

3. Results

3.1. Analysis of Cucurbita pepo L. Seed oil

VOCs determined by headspace solid-phase microextraction coupled to gas chromatography/mass spectrometry (HS-SPME/GC–MS) resulted in the identification of 15 compounds (Supplementary material, Table S1), which had previously been identified in other studies (Bowman and Barringer, 2012; Poehlmann and Schieberle, 2013). In addition, non-volatile compounds were identified in negative and positive MS modes (Supplementary material, Table S2).

3.2. Formulation, optimization and characterization of nanocapsules

Prior to nanocapsule preparation, a group of emulsions was prepared to determine the final HLB of PSO. Characterization and stability results indicated that PSO could be emulsified by the spontaneous method using Tween 20 and Span 80 (data not shown). Emulsions with optimal stability were obtained using these surfactants at a percentage ratio of 35.5 and 64.5, respectively, corresponding to a final HLB 8.7.

NCs were developed using the 2^2 factorial design with central points (0,0). A total of 11 randomized experimental batches (L101–L111) were prepared varying amounts of PSO (11.8 mg, 20 mg, 40 mg, 60 mg and 68.2 mg) and PCL (19.25 mg, 50 mg, 125 mg, 200 mg and 230.75 mg) in accordance with the factorial design. Particle size, PDI and zeta potential are described in Table 3. Particle size ranged from 338.9 ± 1.4 nm (L101) to 963.9 ± 70.03 nm (L107). In addition, NCs exhibited surface charges ranging from –23.1 ± 1.08 mV (L108) to –17.9 ± 0.95 mV (L101). Still, acceptable PDI values (from 0.15 to 0.36) were observed in this group of formulations. By using the quadratic statistical model, the response surface methodology was applied to the size values obtained from the 11 batches of the factorial design (Fig. 2A). Macroscopic analysis revealed fluid nanosuspensions exhibiting a homogenous milky-white aspect with no signs of physical instability, e.g. oil droplets or polymer aggregates (Supplementary material, Fig. S1-A).

The mean hydrodynamic diameter of the NC produced was shown to be greatly influenced by different quantities of PCL and PSO, as demonstrated in the Pareto plot shown in Fig. 2B. Considering these data, and in order to obtain improved formulations with minimal amounts of PCL, four additional batches were prepared aiming process optimization (L203, L204, L305 and L307). As a result, the optimized quantities of PSO and PCL for NC preparation were defined as 20 mg of PCL and 87.5 mg of PSO (L307). The resulting particle size and zeta

Table 3
Size and zeta potential of nanocapsules from factorial planning.

Formulation	PCL	PSO	Size (nm)	PDI	Zeta Potential (mV)
L101	−1.0	−1.0	338.9 ± 1.40	0.15 ± 0.03	−17.9 ± 0.95
L102	−1.0	1.0	427.2 ± 3.19	0.26 ± 0.01	–22.9 ± 1.31
L103	1.0	−1.0	526.5 ± 8.56	0.22 ± 0.03	−18.8 ± 0.58
L104	1.0	1.0	499.0 ± 9.70	0.28 ± 0.03	−20.1 ± 1.27
L105	−1.4	0.0	404.9 ± 7.61	0.19 ± 0.01	−18.5 ± 0.61
L106	1.4	0.0	639.9 ± 2.73	0.21 ± 0.01	−19.3 ± 0.20
L107	0.0	−1.4	963.6 ± 70.03	0.36 ± 0.03	−19.4 ± 0.92
L108	0.0	1.4	410.6 ± 9.54	0.34 ± 0.07	–23.1 ± 1.08
L109	0.0	0.0	509.0 ± 11.89	0.23 ± 0.06	−20.2 ± 0.94
L110	0.0	0.0	537.7 ± 4.49	0.23 ± 0.01	−20.7 ± 1.55
L111	0.0	0.0	543.0 ± 11.91	0.21 ± 0.03	−20.1 ± 1.25
L203	−1.0	1.5	418.5 ± 20.45	0.26 ± 0.04	−27.1 ± 0.51
L204	−1.0	0.0	468.4 ± 9.67	0.26 ± 0.01	−14.4 ± 0.32
L305	0.0	1.0	400.7 ± 6.76	0.32 ± 0.00	−12.1 ± 0.83
L307	−1.0	−0.5	403.4 ± 5.38	0.13 ± 0.03	−13.5 ± 1.22

L101-L111: Factorial planning 2^2; L203-L307: Optimization of formulations.

potential of the optimized NC-IVM formulation were 403.4 ± 5.38 nm and –13.5 ± 1.22, respectively. Of note, this formulation exhibited the lowest PDI value (0.13 ± 0.03) with monomodal particle size distribution. The morphology of NC-IVM was assessed by transmission electron microscopy (TEM), indicating NC uniformity and spherical structures measuring approximately 400 nm in diameter (Fig. 3). Still, TEM micrographs revealed homogeneous and dispersed nanocapsules with minor aggregation. The particle size was further supported by TEM images, reflecting a direct association with light scattering measurements.

3.3. IVM solubility and partition coefficient

To investigate the entrapment of IVM in the proposed nanosystem, drug solubility and partition coefficient were determined. IVM solubility in PSO reached 4266.5 ± 38.6 μg/mL in PSO. Consistent with the solubility results, the determined partition coefficient of IVM in PSO/water (logP) was 2.44.

3.4. Encapsulation efficiency

Formulations loaded with IVM (from L401 to L406) showed similar particle size, surface charge, and encapsulation efficiency (ca. 100.0%) (Table 4). Variations in oil phase to drug ratio did not significantly affect the resulting nanoparticle size and zeta potential values, with the exception of the L407. For this formulation, the higher IVM content in the oil core increased particle size and surface charge significantly. Accordingly, it is reasonable to assume that L406 is the formulation capable of encapsulating IVM with optimal properties. Thus, further experiments were performed using this NC-IVM formulation and the corresponding non-loaded nanocapsules as control (L307). The visual appearance of empty nanocapsules and those containing IVM was similar, presenting as homogeneous and fluid suspensions with no evidence of instability as observed by naked eye (Supplementary material, Fig. S1-B).

3.5. Long-term stability of nanocapsules

Nanosuspensions were monitored at 25 °C and 4 °C over a period of 180 days. Minor variations in particle size and polydispersity were observed for blank and IVM-loaded nanocapsules. Interestingly, the particle size of nanocapsules did not significantly changed following storage at 25 °C or 4 °C for 180 days (Supplementary material, Tables S4 and S5). The drug content did not change during the stability studies (29.1 ± 0.2 mg). These results were consistent with the lack of macroscopic alterations seen upon visual inspection after 180 days of storage.

3.6. Cell viability testing

The cytotoxicity of PSO-PCL nanocapsules was assessed through *in vitro* viability testing. Assays showed the ability of nanocapsules to mitigate IVM toxicity in L929 fibroblasts and J774 macrophages. Both cell lines exposed to the IVM-loaded nanoparticles maintained viability at the two tested concentrations shown in Fig. 4A and B. By contrast, cell viability significantly decreased at higher concentrations of exogenous IVM exposure. This effect was more pronounced in macrophages, resulting in an approximately 70% reduction in cell viability ($p < 0.001$) following treatment with free/non-encapsulated IVM at 0.3 mM. Blank nanocapsules did not induce toxic effects on both cell lines.

3.7. In vitro anthelmintic activity

In order to evaluate the chemotherapeutic potential of NC-IVM compared to free IVM, cultured parasitic adult female worms were exposed to different concentrations of free and nanoencapsulated IVM as described in Materials and Methods. The mortality was observed earlier in the NC-IVM treated group, starting on day 4 (27.8% and 33.3% mortality at 60 and 120 μg/mL, respectively) and reaching 100% on day 6 at all tested concentrations. In contrast, anthelmintic activity was only seen on day 6 using free IVM, with 44.4% of mortality at 120 μg/mL, increasing to 72.2% on day 7. The low dose treatment at 15 μg/mL induced only 38.9% of mortality in the same window of time. In addition, the NC-BL formulation also demonstrated an anti-parasitic effect, as evidenced by 44.4% and 61.1% mortality on day 7 at concentrations of 60 and 120 μg/mL, respectively (Fig. 5 and Supplementary material, Table S6).

To gain insights into the possible mechanisms involved in *Strongyloides* death, bright field microscopy was used to observe female adult worms in response to exposure to different concentrations of NC-IVM compared to controls at different time points. Fig. 6-panel 1 illustrates representative results obtained with 15 μg/mL, and higher concentrations showed similar effects but observed earlier (data not shown). An exacerbated increase in orally secreted adhesive mucosubstance production was observed in NC-IVM and NC-BL treatments (Fig. 6D–I) compared to controls (Fig. 6A and B). In worms treated with free IVM, increased production of mucosubstance was only observed in the first hours after drug exposure (Fig. 6J), but not present at later time points (Fig. 6K). In the group treated with NC-IVM, all females presented vesicle-like structures at 6 days after drug exposure (Fig. 6F); similar structures were not observed in the other groups (Fig. 6C, I and L).

Next, fluorescent-labeled NC-IVM were used together with fluorescence microscopy to trace the distribution of the NCs in parasite internal structures. Intense red fluorescence and vesicle-like structures could be observed inside parasite body six days after treatment with NC-IVM 15 μg/mL (Fig. 6A and B, zoomed region C, D; panel 2) or NC-IVM 60 μg/mL (Fig. 6E and F, zoomed region G and H; panel 2).

4. Discussion

IVM has proved to be very useful for the control of diseases caused by

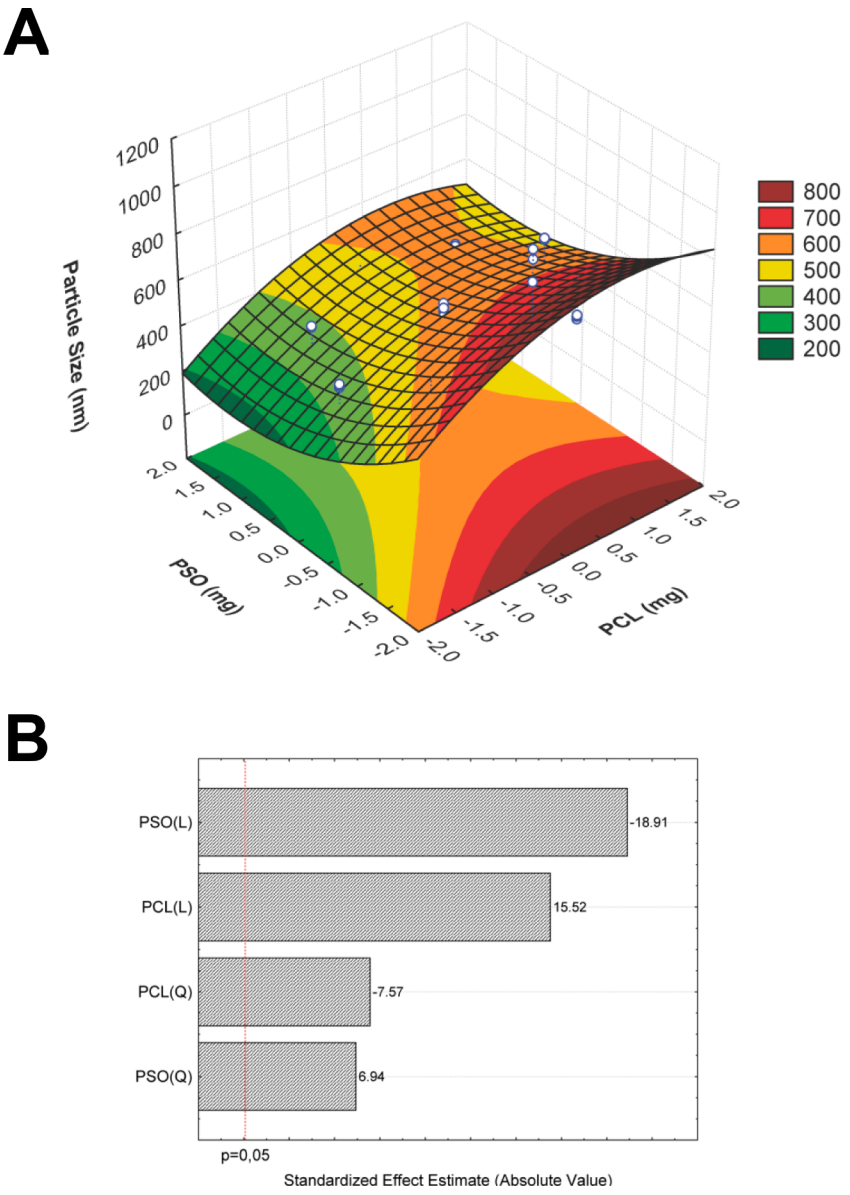

Fig. 2. (A) 3D response surface for size (dependent variable) and independent variables of PCL and PSO for nanocapsules production. (B) Pareto chart with linear (L) and quadratic (Q) standardized effects for the size of the nanocapsules.

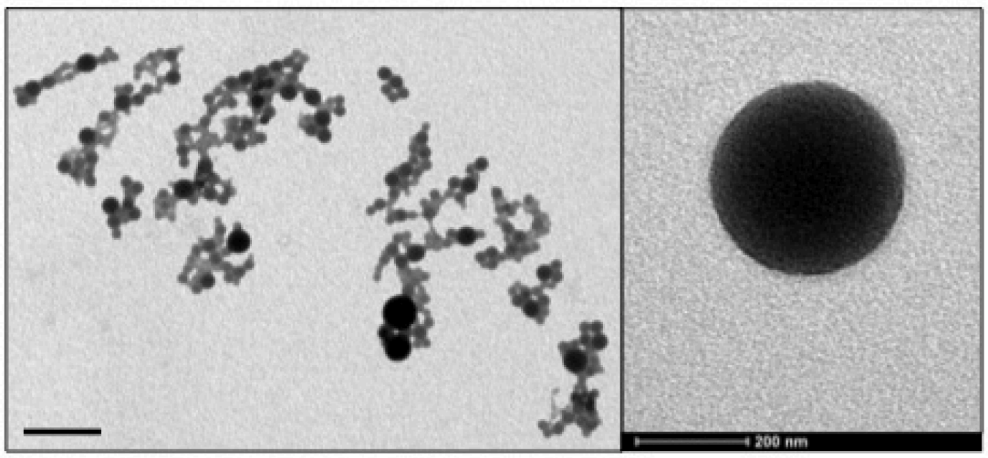

Fig. 3. Transmission electron micrographs of optimized nanocapsules. Magnification bar denotes 1 μm.

Table 4
Characterization data of nanocapsules loaded with IVM.

Formulation	IVM loading (mg)	IVM: PSO ratio	Size (nm)	PDI	Zeta Potential (mV)	EE (%)
L401	4.4	1:20	373.8 ± 10.76	0.096 ± 0.044	−21.7 ± 0.721	100.0
L402	5.8	1:15	425.6 ± 18.75	0.153 ± 0.057	−20.5 ± 0.321	100.0
L403	8.8	1:10	429.0 ± 11.08	0.152 ± 0.017	−21.5 ± 0.666	100.0
L404	17.5	1:5	416.9 ± 16.25	0.157 ± 0.156	−21.3 ± 0.681	100.0
L405	21.9	1:4	417.6 ± 4.76	0.083 ± 0.099	−21.6 ± 0.557	100.0
L406	29.2	1:3	392.9 ± 11.47	0.120 ± 0.068	−23.1 ± 0.503	100.0
L407	43.8	1:2	507.2 ± 10.07*	0.158 ± 0.128	−36.8 ± 0.513*	98.9

IVM:PSO: ivermectin: pumpkin seed oil ratio; PDI: polydispersity index; EE: encapsulation efficiency.
* SD ≤ 1%; *p < 0.05 vs. all formulations.

nematodes, particularly in the treatment of onchocerciasis and strongyloidiasis in humans. However, the clinical value of IVM is limited by formulation challenges, primarily associated to its poor water solubility (Class II – BCS). In fact, there is a lack of appropriate formulations capable of providing improved pharmacokinetics and drug delivery targeting mechanisms. This is a critical issue not only for improving the IVM oral bioavailability against parasitic diseases, but also for accelerating its re-purposing in the context of other pathologies (Formiga et al., 2021). Therefore, novel delivery strategies are needed to optimize IVM bioavailability.

In this study, we sought to develop a novel IVM formulation based on polymer nanocapsules (NCs) formulated with PSO as oil core. The chemical composition of PSO was determined by GC–MS and HRMS analysis. The VOCs presently identified in PSO had already been previously described in other analyses (Bowman and Barringer, 2012; Poehlmann and Schieberle, 2013), and the obtained retention indices were also consistent with previous reports (Babushok et al., 2011). The main VOCs identified in PSO were (E, E) 2,4-decadienal (16.21%), 3-hexanol (13.51%) and (E) −2-tridecanal (6.58%). Matsui et al. were the first to apply GC in PSO analysis, and suggested that the compound (E, E)-2,4-decadienal is an important odorant found in PSO (Matsui et al., 1998). Regarding this complex chemical composition, and in the light of reports about biological properties of pumpkin seeds, it is reasonable to consider that some of these compounds identified in PSO are bioactive agents. Importantly, antiparasitic effects of pumpkin seed bioproducts have been previously described (Feitosa et al., 2013; Grzybek et al., 2016; Beshay et al., 2019), and it could potentially boost the bioactivity of IVM in a synergistic manner.

For the rational design and development of PSO-NCs, we previously determined the critical HLB of PSO. This is relevant for obtaining NCs by the nanoprecipitation method, considering that an oil/water emulsion is formed spontaneously by the polymer interfacial deposition at the interface (Besheer et al., 2009). Thus, the formation of stable oil/water emulsions is crucial for obtaining non-aggregated and well-dispersed nanoparticles, since it positively impacts stability (Sjöström et al., 1995). Herein, the HLB value of PSO was considered to determine the proportions and amounts of each surfactant to be used in nanocapsule formulation. In addition, factorial planning was employed to adjust the quantities of PCL (x_1) and PSO (x_2) for obtaining NCs of smaller size and

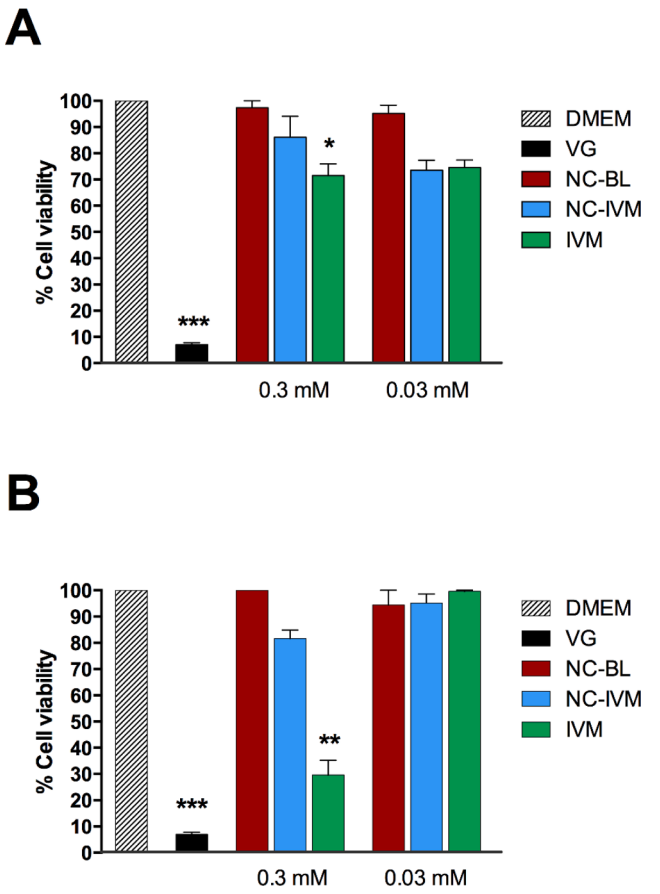

Fig. 4. Cell viability assays by the Alamar Blue colorimetric method in L929 fibroblasts (A) and J774 macrophages (B) exposed to the following treatments: nanocapsules containing ivermectin (NC-IVM) and exogenous/non-encapsulated ivermectin (IVM) at concentrations of 0.3 mM and 0.03 mM. Both cell lines also received blank nanocapsules (NC-BL). DMEM medium served as positive control. Gentian violet solution (VG, pararosaniline chloride at 10 μM) was used as negative control of cell viability. *p < 0.05 and **p < 0.001 vs. NC-IVM; ***p < 0.0001 vs. all treatments and controls. (For interpretation of the references to color in this figure legend, the reader is referred to the web version of this article.)

size distribution capable of carrying greater amounts of oil. Therefore, it was possible to test different PCL/PSO ratios, searching for improved NCs with greater oil incorporation. This could have a positive impact on drug loading due to high IVM solubility in PSO, which could endow the NC-IVM formulation with higher activity against parasites (as will be discussed later).

Indeed, PCL/PSO ratio played a key role on size and size distribution of resulting NCs. The average size of these NCs was strongly influenced by the amounts of PCL and PSO employed, as indicated by the statistically positive effect produced by reductions in the amount of PSO, which resulted in decreased particle size of NCs. Conversely, the opposite effect was produced by PCL. With regard to zeta potential, low molecular weight PCL was used to formulate nanocapsules, which exhibited negative surface charges, corroborating with literature (Lammari et al., 2020). The low to moderate values of zeta potential (from −12.1 to −27.1 mV) could be result from the stabilizing steric mechanism of polysorbate 20 (Tween 20), a nonionic polyoxygenated surfactant (Fiel et al., 2011).

Aiming high drug entrapment into PSO-NCs, IVM solubility and partition coefficient were determined. The solubility of IVM in PSO (4,266.5 ± 38.6 μg/mL) was ~1100-fold higher as compared to free IVM in water (4 μg/mL). Dong and colleagues reported similar results incorporating IVM into soy phosphatidylcholine-sodium deoxycholate

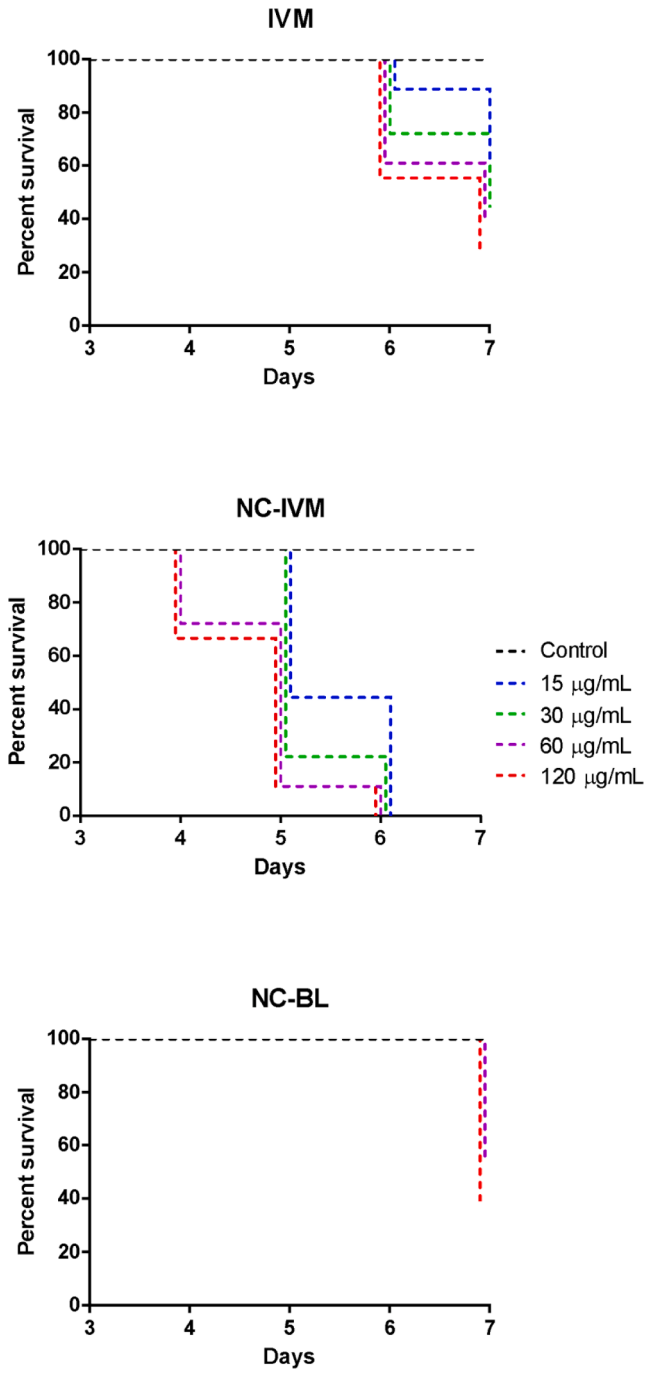

Fig. 5. In vitro effects of NC-IVM on viability of *Strongyloides venezuelensis* female adult worms. Adult worms were treated with different concentrations of NC-IVM, NC-BL or free IVM and mortality accessed at different time points as described in Methods and Kaplan-Meier survival curves were build.

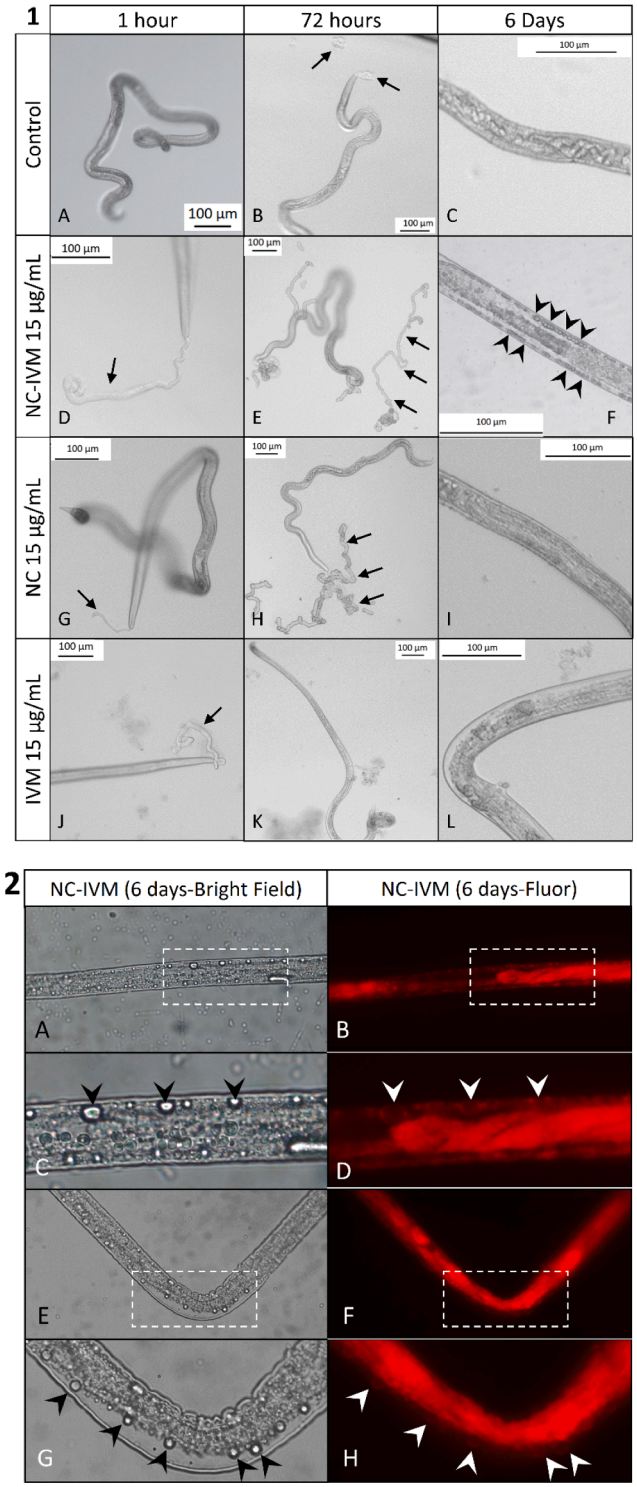

Fig. 6. Panel 1 – Microscopic assessment of *Strongyloides venezuelensis* treated with 15 μg/mL NC-IVM and respective controls at different time points. Bright field microscopy of control adult female worms (A–C), treated with 15 μg/mL of NC-IVM (D–F), NC-BL (G–I) and 15 μg/mL of free IVM (J–L). Plain arrows indicate mucosubstance and head arrows indicate vesicles. Panel 2 – Qualitative assessment of nanoparticle biodistribution by fluorescence imaging in *S. venezuelensis*. Females worms after *in vitro* exposure to NC-IVM labeled with rhodamine (A–D) 15 μg/ml (6 days); (E–F) 60 μg/ml (6 days).

mixed micelles (Dong et al., 2016). This demonstrates favorable characteristics necessary to load high levels of drug into a reservoir surrounded by a polymer wall, in this case an oily nucleus derived from PSO. Moreover, as aforementioned, the combined antiparasitic activity of PSO and IVM is highly desirable in a single formulation.

After formulation optimization with empty NCs (drug-free), IVM was incorporated into the nanosystem. The encapsulation efficiency (EE) achieved 100% without any changes on this parameter with the increase on IVM content (L401–L406). However, variations were observed after the introduction of 43.8 mg of IVM into formulation (L407). Similarly, no significant shifts on particle size, size distribution and zeta potential

were detected with IVM:PSO ratio between 1:20 and 1:3. It seems reasonable to suppose that an IVM:PSO ratio as from 1:2 begins negatively to affect the nanosystem. As evidence of this, L407 formulation presented significant increases on size and zeta potential values. Still, encapsulation efficiency was no longer more 100%. Therefore, high IVM entrapment efficiency into the NCs was dependent of the drug concentration into the organic phase.

In fact, upon increasing the drug concentration in the organic phase, the entrapment efficiency increases to a point and thus begins to decline due to complete consumption of polymer available to encapsulate the drug. Then, the drug remains un-entrapped and there is a decrease in entrapment efficiency based on the initial amount of drug taken for formulation preparation (Debnath et al., 2017; Chishti et al., 2019). In turn, some factors probably contributed to high entrapment of IVM into PCL-PSO nanocapsules such the high lipophilicity of IVM (Log P = 3.217), the high solubility of IVM in PSO, and its solubility in acetone. Collectively, these factors lead to low diffusivity of IVM in water. Consequently, most of the drug remained in the organic phase with the polymer until the nanocapsule formation. In the context of development of a new formulation of IVM, high encapsulation efficiency into micro- and nanocarriers is conveniently attractive, and our results are comparable or even better to previous studies. For example, the EE of IVM in lipid nanocapsules was higher than 90% and did not change over time, suggesting the physical stability of these nanocarriers (Ullio-Gamboa et al., 2016). Moreover, Ali and colleagues investigating PLGA nanoparticles containing IVM for antifilarial chemotherapy found high EE values (Ali et al., 2014). Similarly, incorporating IVM into PLGA and PLA-based microparticles, Camargo et al. found high levels of drug entrapment (>90%) (Camargo et al., 2010). In an elegant strategy, Surnar and colleagues reported high %EE of IVM in polymeric nanoparticles of poly(lactide-co-glycolide)-b-poly-ethylene glycol (PLGA-b-PEG) block copolymers intended for application in Zika virus therapy (Surnar et al., 2019). Another study reported IVM encapsulation efficiency in the 67.37 and 84.91% range into microspheres based on poly (d,l-lactide) and poly-(ε-caprolactone) prepared by the emulsion solvent evaporation method (Dorati et al., 2015).

With regard to long-term stability, no significant increases on particle size were observed in either NC-BL or NC-IVM, and PDI values remained stable over 180 days, suggesting the stability of the PSO/PCL system. Indeed, the incorporation of IVM did not introduce any physical instability in developed nanocapsules, according to data collected during the monitoring time (Table S5). Correlating with these findings, drug-containing formulations remained macroscopically identical to formulations without IVM, with visual appearance similar to that observed just after preparation. All formulations maintained a milky-white aspect without color change or any signs of instability (coalescence, creaming, flocculation, sedimentation, etc.). These results indicate that the optimized formulation remains stable over time, offering a suitable shelf-life.

The cytocompatibility of nanoformulated IVM was demonstrated by cell viability assays. Significant reductions on cell viability were detected in both macrophages and fibroblasts exposed to the highest concentration of free IVM, with more pronounced effect in macrophages. On the other hand, PCL-PSO nanocapsules were able to mitigate possible cytotoxic effects of IVM at the same concentration (0.3 mM). Therefore, these data suggested favorable interactions between cells and PCL-PSO nanocapsules in their capacity to deliver IVM, exerting protective effects.

The *in vitro* evaluation of the anthelmintic action of the produced nanocapsules was performed in *S. venezuelensis*. This parasitic nematode has been used as a model to study the parasite-host relationship in human and animal strongyloidiasis (Marra et al., 2011). IVM, the drug of choice for the treatment of strongyloidiasis, is typically employed as a positive control in experiments involving these nematodes (Rodrigues and Thesis, 2017). Our results demonstrated higher efficacy for NC-IVM compared to free IVM, with earlier mortality seen at lower dosages.

Interestingly, an exacerbated amount of mucosubstances was produced by parasites treated with NC-BL and NC-IVM. These secretions contain adhesive molecules that form insoluble complexes, and are normally secreted by parasitic females of *S. venezuelensis* (Maruyama and Nawa, 1997). Mucosubstances are considered a key aspect in the ability of parasites to survive in the host, likely due to participation in worm attachment to the intestinal epithelium and the construction of worm tunnel walls in the mucosal epithelial layer where they become lodged (Maruyama and Nawa, 1997). As reactivity to these substances has been documented in the sera of infected rats, it is possible that higher amounts may lead to a more intense immune response that facilitates parasite elimination (Maruyama and Nawa, 1997; Maruyama et al., 2003). This secretome was recently characterized and included proteins previously identified to be involved in parasitism in other helminths, as well as proteins unique to *S. venezuelensis* (Maeda et al., 2019). The formation of vesicles was an unexpected finding, which warrants further investigation.

Efforts to correlate the anthelmintic action of NC-IVM with its kinetic release profile were pursued in this study. NC-IVM exhibited negligible drug release, with only 2.5% of encapsulated drug released in 7 days under sink conditions in PBS pH 7.4 with 2% Tween 80 (data not shown). However, effective antithelmintic activity was demonstrated in the same period, with the nanocapsules internalized into the worms. In the *in vivo* microenvironment of parasite body, a faster water and drug molecule mass transfer throughout the polymer matrix may occur, and disintegration of nanocapsules could led to a faster release of ivermectin. These findings should support further *in vivo* investigation to determine the effects IVM nanocapsules in a rodent model of Strongyloides infection via oral gavage (Mendonça et al., 2019).

5. Conclusion

The present investigation describes the first encapsulation of IVM in PCL nanocapsules formulated with a PSO oily core. The developed protocol was found to produce a feasible, non-toxic and stable novel IVM nanotherapeutic. The optimized formulation demonstrated to possess *in vitro* a higher anti-*Strongyloides* activity compared to the free drug. Collectively, these findings demonstrate the potential of this nanoformulation approach to enhance the anti-parasitic effects of IVM, and possibly, to reduce secondary effects associated with this drug.

Declarations

Author contributions The manuscript was written through contributions of all authors. All authors have given approval to the final version of the manuscript.

Funding This work was supported by grants from the Fundação de Amparo à Ciência e Tecnologia do Estado de Pernambuco – FACEPE (APQ-0443-4.03/18), the Programa Inova FIOCRUZ (VPPIS-005-FIO-20-2-22; VPPIS-004-FIO-22) and the Programa de Fortalecimento Acadêmico – PFA/UPE (APQ 2018-2020). This study was also financed in part by the Coordenação de Aperfeiçoamento de Pessoal de Nível Superior – Brasil (CAPES) – Finance Code 001.

CRediT authorship contribution statement

Zilyane Cardoso de Souza: Investigation, Methodology, Formal analysis, Data curation, Visualization, Writing – original draft, Writing – review & editing. **Francisco Humberto Xavier Júnior:** Investigation, Methodology, Formal analysis, Supervision, Writing – original draft, Writing – review & editing. **Irapuan Oliveira Pinheiro:** Investigation, Methodology, Resources, Supervision. **Juliana de Souza Rebouças:** Investigation, Methodology, Resources, Supervision, Writing – review & editing. **Brenda Oliveira de Abreu:** Investigation, Methodology, Visualization, Formal analysis. **Paulo Roberto Ribeiro Mesquita:** Investigation, Methodology, Visualization, Formal analysis. **Frederico de Medeiros Rodrigues:** Investigation, Methodology, Visualization, Formal analysis. **Helenita Costa Quadros:** Investigation, Methodology,

Visualization, Formal analysis. **Tiago Manuel Fernandes Mendes:** Investigation, Methodology, Visualization, Formal analysis. **Paul Nguewa:** Conceptualization, Writing – original draft. **Silmara Marques Allegretti:** Conceptualization, Investigation, Methodology, Resources, Supervision, Formal analysis, Writing – original draft. **Leonardo Paiva Farias:** Conceptualization, Investigation, Methodology, Formal analysis, Writing – original draft, Writing – review & editing. **Fabio Rocha Formiga:** Conceptualization, Investigation, Methodology, Resources, Supervision, Formal analysis, Writing – original draft, Writing – review & editing.

Declaration of Competing Interest

The authors declare that they have no known competing financial interests or personal relationships that could have appeared to influence the work reported in this paper.

Data availability

Data will be made available on request.

Acknowledgements

ZCS would like to thank FACEPE for doctoral scholarship (IBPG-0699-2.10/16). FRF holds a productivity fellowship (CNPq 313931/2021-6). PN thanks Fundación La Caixa (LCF/PR/PR13/11080005), Fundación Caja Navarra, Fundación Roviralta, Ubesol, Government of Navarre, Laser Ebro, Inversiones Garcilaso de la Vega and COST Actions CA18217 (ENOVAT) and CA18218, and EU Project unCoVer (DLV-101016216) for their support. The authors are grateful to Andris K. Walter for critical manuscript review and English language copyediting services.

Appendix A. Supplementary material

Supplementary data to this article can be found online at https://doi.org/10.1016/j.ijpharm.2023.122965.

References

Ali, M., Afzal, M., Verma, M., Misra-Bhattacharya, S., Ahmad, F.J., Dinda, A.K., 2013. Improved antifilarial activity of ivermectin in chitosan-alginate nanoparticles against human lymphatic filarial parasite. Brugia Malayi Parasitol. Res. 112, 2933 2943.

Ali, M., Afzal, M., Verma, M., Bhattacharya, S.M., Ahmad, F.J., Samim, M., Abidin, M.Z., Dinda, A.K., 2014. Therapeutic efficacy of poly (lactic-co-glycolic acid) nanoparticles encapsulated ivermectin (nano-ivermectin) against brugian filariasis in experimental rodent model. Parasitol. Res. 113, 681–691. https://doi:10.1007/s00436-013-3696-5.

Amato-Neto, V., Carignani, F.L., Matsubara, L., Braz, L.M., 1997. The treatment of rats experimentally infected with Strongyloides venezuelensis by orally administered ivermectin. Rev. Soc. Bras. Med. Trop. 30, 481 484.

Babushok, V.I., Linstrom, P.J., Zenkevich, I.G., 2011. Retention indices for frequently reported compounds of plant essential oils. J. Phys. Chem. Ref. Data. 40, 043101 https://doi.org/10.1063/1.3653552.

Beshay, E.V.N., Rady, A.A., Afifi, A.F., Mohamed, A.H., 2019. Schistosomicidal, antifibrotic and antioxidant effects of Cucurbita pepo L. seed oil and praziquantel combined treatment for Schistosoma mansoni infection in a mouse model. J. Helminthol. 93, 286–294. https://doi:10.1017/S0022149X18000317.

Besheer, A., Vogel, J., Glanz, D., Kressler, J., Groth, T., Mäder, K., 2009. Characterization of PLGA nanospheres stabilized with amphiphilic polymers: hydrophobically modified hydroxyethyl starch vs pluronics. Mol. Pharm. 6, 407–415. https://doi:10.1021/mp800119h.

Bisoffi, Z., Buonfrate, D., Montresor, A., Requena-Méndez, A., Muñoz, J., Krolewiecki, A. J., Gotuzzo, E., Mena, M.A., Chiodini, P.L., Anselmi, M., Moreira, J., Albonico, M., 2013. Strongyloides stercoralis: a plea for action. PLoS Negl. Trop. Dis. 7.

Bowman, T., Barringer, S., 2012. Analysis of factors affecting volatile compound formation in roasted pumpkin seeds with selected ion flow tube-mass spectrometry (SIFT-MS) and sensory analysis. J. Food Sci. 77, C51–C60. https://doi:10.1111/j.1750-3841.2011.02465.x.

Burnham, G., Mebrahtu, T., 2004. The delivery of ivermectin (Mectizan). Trop. Med. Int. Health 9, A26–A44.

Caly, L., Druce, J.D., Catton, M.G., Jans, D.A., Wagstaff, K.M., 2020. The FDA-approved drug Ivermectin inhibits the replication of SARS-CoV-2 in Vitro. Antiviral Res. 178, 104787 https://doi.org/10.1016/j.antiviral.2020.104787.

Camargo, J.A., Sapin, A., Daloz, D., Maincent, P., 2010. Ivermectin-loaded microparticles for parenteral sustained release: in vitro characterization and effect of some formulation variables. J. Microencapsul. 27, 609–617. https://doi:10.3109/02652048.2010.501397.

Chaves, P.S., Ourique, A.F., Frank, L.A., Pohlmann, A.R., Guterres, S.S., Beck, R.C.R., 2017. Carvedilol-loaded nanocapsules: Mucoadhesive properties and permeability across the sublingual mucosa. Eur. J. Pharm. Biopharm. 114, 88–95. http://doi:10.1016/j.ejpb.2017.01.007.

Chen, C.K., Law, W.C., Aalinkeel, R., Yu, Y., Nair, B., Wu, J., Mahajan, S., Reynolds, J.L., Li, Y., Lai, C.K., Tzanakakis, E.S., Schwartz, S.A., Prasad, P.N., Cheng, C., 2014. Biodegradable cationic polymeric nanocapsules for overcoming multidrug resistance and enabling drug-gene co-delivery to cancer cells. Nanoscale. 6, 1567–1572. https://doi:10.1039/c3nr04804g.

Chishti, N., Jagwani, S., Dhamecha, D., Jalalpure, S., Dehghan, M.H., 2019. Preparation, optimization, and in vivo evaluation of nanoparticle-based formulation for pulmonary delivery of anticancer drug. Medicina. 55, 294. https://doi.org/10.3390/medicina55060294.

Clark, S.L., Crowley, A.J., Schmidt, P.G., Donoghue, A.R., Piché, C.A., 2004. Long-term delivery of ivermectin by use of poly(D, L-lactic-co-glycolic)acid microparticles in dogs. Am. J. Vet. Res. 65, 752–757. https://doi:10.2460/ajvr.2004.65.752.

Croci, R., Bottaro, E., Chan, K.W., Watanabe, S., Pezzullo, M., Mastrangelo, E., Nastruzzi, C., 2016. Liposomal systems as nanocarriers for the antiviral agent Ivermectin. Int. J. Biomater. 8043983. https://doi:10.1155/2016/8043983.

Debnath, S.K., Saisivam, S., Omri, A., 2017. PLGA Ethionamide nanoparticles for pulmonary delivery: development and in vivo evaluation of dry powder inhaler. J. Pharm. Biomed. Anal. 145, 854–859. https://doi:10.1016/j.jpba.2017.07.051.

Dong, J., Song, X., Lian, X., Fu, Y., Gong, T., 2016. Subcutaneously injected ivermectin-loaded mixed micelles: formulation, pharmacokinetics and local irritation study. Drug Deliv. 23, 2220–2227. https://doi:10.3109/10717544.2014.956849.

Dorati, R., Genta, I., Colzani, B., Modena, T., Bruni, G., Tripodo, G., Conti, B., 2015. Stability evaluation of ivermectin-loaded biodegradable microspheres. AAPS PharmSciTech. 16, 1129–1139. https://doi:10.1208/s12249-015-0305-1.

Feitosa, T.F., Vilela, V.L.R., Athayde, A.C.R., Braga, F.R., Dantas, E.S., Vieira, V.D., Melo, L.R.B., 2013. Anthelmintic efficacy of pumpkin seed (Cucurbita pepo Linnaeus, 1753) on ostrich gastrointestinal nematodes in a semiarid region of Paraíba State, Brazil. Trop. Anim. Health Prod. 45, 123–127. https://doi:10.1007/s11250-012-0182-5.

Fessi, H., Puisieux, F., Devissaguet, J.P., 1988. Procédé de preparation dès systèmes coloïdaux d'une substance sous forme de nanocapsules. Europ. Patent. 0274961 A1.

Fiel, L.A., Rebêlo, L.M., Santiago, T.M., Adorne, M.D., Guterres, S.S., Sousa, J.S., Pohlmann, A.R., 2011. Diverse deformation properties of polymeric nanocapsules and lipid-core nanocapsules. Soft Matter. 7, 7240–7247. https://doi.org/10.1039/C1SM05508A.

Formiga, F.R., Leblanc, R., Rebouças, J.S., Farias, L.P., Oliveira, R.N., Pena, L., 2021. Ivermectin: an award-winning drug with expected antiviral activity against COVID-19. J. Control. Release. 329, 758–761.

Frank, L.A., Contri, R.V., Beck, R.C.R., Pohlmann, A.R., Guterres, S.S., 2015. Improving drug biological effects by encapsulation into polymeric nanocapsules. Wiley Interdiscip. Rev. Nanomed. Nanobiotechnol. 7, 623–639. https://doi:10.1002/wnan.1334.

Gokbulut, C., Karademir, U., Boyacioglu, M., McKellar, Q.A., 2006. Comparative plasma dispositions of ivermectin and doramectin following subcutaneous and oral administration in dogs. Vet. Parasitol. 135, 347–354.

González-Canga, A., Prieto, A.M.S., Liébana, M.J.D., Martínez, N.F., Vega, M.S., Vieitez, J.J.G., 2009. The pharmacokinetics and metabolism of ivermectin in domestic animal species. Vet. J. 179, 25–37.

Grzybek, M., Kukula-Koch, W., Strachecka, A., Jaworska, A., Phiri, A.M., Paleolog, J., Tomczuk, K., 2016. Evaluation of anthelmintic activity and composition of pumpkin (Cucurbita pepo L.) seed extracts-in vitro and in vivo studies, 1456 Int. J. Mol. Sci. 17. https://doi:10.3390/ijms17091456.

Kaplan, R.M., Vidyashankar, A.N., 2012. An inconvenient truth: global worming and anthelmintic resistance. Vet. Parasitol. 186, 70 78.

Laing, R., Gillan, V., Devaney, E., 2017. Ivermectin - old drug, new tricks? Trends Parasitol. 33, 463–472.

Lammari, N., Louaer, O., Meniai, A.H., Elaissari, A., 2020. Encapsulation of essential oils via nanoprecipitation process: overview, progress, challenges and prospects. Pharmaceutics. 12, 431. https://doi:10.3390/pharmaceutics12050431.

Luvira, V., Watthanakulpanich, D., Pittisuttithum, P., 2014. Management of Strongyloides stercoralis: a puzzling parasite. Int. Health. 6, 273 281.

Lv, C., Liu, W., Wang, B., Dang, R., Qiu, L., Ren, J., Yan, C., Yang, Z., Wang, X., 2018. Ivermectin inhibits DNA polymerase UL42 of pseudorabies virus entrance into the nucleus and proliferation of the virus in vitro and vivo. Antiviral Res. 159, 55–62. https://doi.org/10.1016/j.antiviral.2018.09.010.

Macedo, J.P., Fernandes, L.L., Formiga, F.R., Reis, M.F., Nagashima Júnior, T., Soares, L. A.L., Egito, E.S.T., 2006. Micro-emultocrit technique: a valuable tool for determination of critical HLB value of emulsions. AAPS PharmSciTech. 7, E146–E152. https://doi:10.1208/pt070121.

Maeda, Y., Palomares-Rius, J.E., Hino, A., Afrin, T., Mondal, S.I., Nakatake, A., Maruyama, H., Kikuchi, T., 2019. Secretome analysis of *Strongyloides venezuelensis* parasitic stages reveals that soluble and insoluble proteins are involved in its parasitism. Parasit. Vectors. 12, 21. https://doi:10.1186/s13071-018-3266-x.

Marra, N.M., Chiuso-Minicucci, F., Machado, G.C., Zorzella-Pezavento, S.F.G., França, T. G.D., Ishikawa, L.L.W., Amarante, A.F.T., Sartori, A., Amarante, M.R.V., 2011.

Migratory route of Strongyloides venezuelensis in Lewis rats: comparison of histological analyses and PCR. Exp. Parasitol. 127, 334–339. https://doi.org/10.1016/j.exppara.2010.08.006.

Maruyama, H., El-Malky, M., Kumagai, T., Ohta, N., 2003. Secreted adhesion molecules of Strongyloides venezuelensis are produced by oesophageal glands and are components of the wall of tunnels constructed by adult worms in the host intestinal mucosa. Parasitology. 126, 165–171. https://doi:10.1017/s0031182002002718.

Maruyama, H., Nawa, Y., 1997. Strongyloides venezuelensis: adhesion of adult worms to culture vessels by orally secreted mucosubstances. Exp. Parasitol. 85, 10–15. https://doi:10.1006/expr.1996.4100.

Matsui, T., Guth, H., Grosch, W., 1998. A comparative study of potent odorants in peanut, hazelnut, and pumpkin seed oils on the basis of aroma extract dilution analysis (AEDA) and gas chromatography-olfactometry of headspace samples (GCOH) 100. Eur. J. Lipid Sci. Tech. 100, 51–56. https://doi.org/10.1002/(SICI)1521-4133(199802)100:2<51::AID-LIPI51>3.0.CO;2-W.

Mendonça, J.C., Gama, L.A., Hauschildt, A.T., Corá, L.A., Américo, M.F., 2019. Gastrointestinal effects of ivermectin treatment in rats infected with Strongyloides venezuelensis. Acta Trop. 194, 69–77. https://doi.org/10.1016/j.actatropica.2019.03.024.

Montgomery, D.C., 2012. Design and Analysis of Experiments, 8th ed. John Wiley & Sons, New Jersey.

Onoue, S., Yamada, S., Chan, H.K., 2014. Nanodrugs: pharmacokinetics and safety. Int. J. Nanomed. 9, 1025 1037.

Ottesen, E.A., Campbell, W.C., 1994. Ivermectin in human medicine. J. Antimicrob. Chemother. 34, 195–203.

Pacqué, M., Muñoz, B., Greene, B.M., Taylor, H.R., 1991. Community-based treatment of onchocerciasis with ivermectin: safety, efficacy, and acceptability of yearly treatment. J. Infect. Dis. 163, 381 385.

Page, W., Judd, J.A., Bradbury, R.S., 2018. The unique life cycle of Strongyloides stercoralis and implications for public health action. Trop. Med. Infect. Dis. 3, 53–64.

Panic, G., Duthaler, U., Speich, B., Keiser, J., 2014. Repurposing drugs for the treatment and control of helminth infections. Int. J. Parasitol. Drugs Drug Resist. 4, 185 200.

Poehlmann, S., Schieberle, P., 2013. Characterization of the aroma signature of styrian pumpkin seed oil (Cucurbita pepo subsp. pepo var. Styriaca) by molecular sensory science. J. Agric. Food Chem. 61, 2933–2942. https://doi:10.1021/jf400314j.

Poletto, F.S., Beck, R.C.R., Guterres, S.S., Pohlmann, A.R., 2011. Polymeric nanocapsules: concepts and applications. In: Beck, R.C.R., Guterres, S.S., Pohlmann, A.R. (Eds.), Nanocosmetics and Nanomedicines: New Approaches for Skin Care. Springer-Verlag, Berlin Heidelberg, pp. 49–68 https://10.1007/978-3-642-19792-5.

Rodrigues, J.P., Thesis, M., 2017. Avaliação *in vitro* da atividade antihelmíntica da toxina BnSP-6 contra *Strongyloides venezuelensis* e seu rastreamento utilizando CdSe/CdS Magic Sized Quantum Dots. Dissertação (Mestrado em Imunologia e Parasitologia Aplicadas). Universidade Federal de Uberlândia, Uberlândia.

Rugai, E., Mattos, T., Brisola, A.P., 1954. A new technic for the isolation of nematode larvae from feces; modification of Baermann's method. Rev. Inst. Adolfo Lutz. 14, 5–8.

Sjöström, B., Kaplun, A., Talmon, Y., Cabane, B., 1995. Structures of nanoparticles prepared from oil-in-water emulsions. Pharm. Res. 12, 39–48. https://doi.org/10.1023/A:1016278302046.

Surnar, B., Kamran, M.Z., Shah, A.S., Basu, U., Kolishetti, N., Deo, S., Jayaweera, D.T., Daunert, S., Dhar, S., 2019. Orally administrable therapeutic synthetic nanoparticle for Zika virus. ACS Nano. 13, 11034–11048. https://doi:10.1021/acsnano.9b02807.

Takano, R., Sugano, K., Higashida, A., Hayashi, Y., Machida, M., Aso, Y., Yamashita, S., 2006. Oral absorption of poorly water-soluble drugs: computer simulation of fraction absorbed in humans from a miniscale dissolution test. Pharm. Res. 23, 1144–1156. https://10.1007/s11095-006-0162-4.

Ullio-Gamboa, G.V., Palma, S.D., Lifschitz, A., Ballent, M., Lanusse, C., Passirani, C., Benoit, J.P., Allemandi, D.A., 2016. Ivermectin-loaded lipid nanocapsules: toward the development of a new antiparasitic delivery system for veterinary applications. Parasitol. Res. 115, 1945–1953. https://doi:10.1007/s00436-016-4937-1.

Ullio-Gamboa, G., Palma, S., Benoit, J.P., Allemandi, D., Picollo, M.I., Toloza, A.C., 2017. Ivermectin lipid-based nanocarriers as novel formulations against head lice. Parasitol Res. 116, 2111 2117.

Van Voorhis, W.C., van Huijsduijnen, R.H., Wells, T.N.C., Campbell, Profile of William C., Ōmura, Satoshi, Youyou, Tu, 2015. 2015 Nobel laureates in physiology or medicine. Proc. Natl. Acad. Sci. USA 112 (2015), 15773–15776.

Varghese, F.S., Kaukinen, P., Glasker, S., Bespalov, M., Hanski, L., Wennerberg, K., Kummerer, B.M., Ahola, T., 2016. Discovery of berberine, abamectin and ivermectin as antivirals against chikungunya and other alphaviruses. Antiviral Res. 126, 117–124. https://doi.org/10.1016/j.antiviral.2015.12.012.

Xavier-Junior, F.H., Egito, E.S.T., Morais, A.R.V., Alencar, E.N., Maciuk, A., Vauthier, C., 2018. Experimental design approach applied to the development of chitosan coated poly(isobutylcyanoacrylate) nanocapsules encapsulating copaiba oil. Colloids Surf. A Physicochem. Eng. Asp. 536, 251–258. https://doi.org/10.1016/j.colsurfa.2017.02.055.

Yang, S.N.Y., Atkinson, S.C., Wang, C., Lee, A., Bogoyevitch, M.A., Borg, N.A., Jans, D.A., 2020. The broad spectrum antiviral ivermectin targets the host nuclear transport importin alpha/beta1 heterodimer. Antiviral Res. 177, 104760 https://doi.org/10.1016/j.antiviral.2020.104760.